Research Article | Vol. 12, No. 12 / 1 Dec 2021 / Biomedical Optics Express 7673
Biomedical Optics EXPRESS

Detection of carbamazepine in saliva based on surface-enhanced Raman spectroscopy

NING CHEN,[1] YANBING YUAN,[1] PING LU,[1] LUYAO WANG,[1] XUEDIAN ZHANG,[1,2] HUI CHEN,[1] AND PEI MA[1,*]

[1]Key Laboratory of Optical Technology and Instrument for Medicine, Ministry of Education, College of Optical-Electrical and Computer Engineering, University of Shanghai for Science and Technology, Shanghai 200093, China
[2]Shanghai Institute of Intelligent Science and Technology, Tongji University, Shanghai 200092, China
*peima@usst.edu.cn

Abstract: Carbamazepine (CBZ) is a commonly used drug for the treatment of epilepsy. Due to the narrow effective range, CBZ concentration was usually monitored with blood draw from patients. Frequent blood draw is inconvenient and causes physical and psychological pain. Therefore, highly-sensitive, rapid, label-free, and non-invasive drug detection methods can be alternatives to bring a relief. In this work, we have proposed a method for the non-invasive detection of CBZ using surface-enhanced Raman spectroscopy (SERS). Gold-silver core-shell nanomaterial substrates were prepared and optimized. Salivary CBZ concentration was measured with SERS as a non-invasive alternative to blood draw. The results showed that there was a linear relationship between SERS response and CBZ concentration in the entire measured range of 10^{-1} $\sim 10^{-8}$ mol/L. The detection limit of this method was 1.26×10^{-9} mol/L. Satisfactory repeatability and stability were also demonstrated. Due to its high sensitivity and ease of operation, the proposed method can serve as an alternative to blood draw for non-invasively monitoring CBZ concentration. It also has great potentials in many other applications of biomedical sciences.

© 2021 Optical Society of America under the terms of the OSA Open Access Publishing Agreement

1. Introduction

Epilepsy is a chronic disease that requires long-term drug treatment. Carbamazepine(CBZ) is a common drug in the treatment of epilepsy, with significant therapeutic effect [1]. However, the effective treatment concentration range of CBZ is narrow, only 4 ~ 12 μg/mL (plasma concentration) [2]. If the concentration is lower than the minimum effective concentration, there would not be any therapeutic effect. If the concentration exceeds the maximum of the range, toxic reaction may occur. In order to improve the safety and effectiveness of CBZ, individualized medication should be implemented to avoid adverse drug reactions, and routine blood concentration detection is usually carried out during CBZ use. However, long-term and frequent blood sample collection brings injury and physical pain to patients. In fact, this is a common issue of chronic drug use [3]. Therefore, a method of monitoring drug concentrations without pain can be a great relief for patients when using drugs such as CBZ.

Although blood tests are gold-standard, saliva may be a good candidate in replacing blood test in chronic disease monitoring. Saliva tests have the advantages of fast, convenient storage and transportation, non-invasive and painless collection, no requirement for medical personnel, and no gender collection problem [4–7]. Most importantly, the salivary concentration of drugs is usually correlated with the plasma concentration. Most drugs appear to pass from blood into the saliva through simple passive diffusion [8]. Generally, alkaline and non-polar molecules with low protein binding and low molecular weight have high lipid solubility and high transmittance of drug transmembrane transport, so they are ideal candidates for salivary monitoring [9]. Compounds such as amphetamines, opioids and cocaine are often found in higher concentrations in oral liquids than in plasma [10]. Other drugs in the oral liquid usually presents a lower concentration

#440939 https://doi.org/10.1364/BOE.440939
Journal © 2021 Received 25 Aug 2021; revised 18 Oct 2021; accepted 20 Oct 2021; published 18 Nov 2021

Biomedical Optics EXPRESS

than in the plasma [11]. For example, the concentration of CBZ in plasma has a good correlation with the concentration of CBZ in saliva, and the concentration of CBZ in saliva was reported to be approximately one-fourth of that in plasma [12]. An obvious challenge of drug detection in oral fluids is to reach the necessary low detection limits. Laboratory analysis usually involves the use of detection methods such as high-performance liquid chromatography (HPLC), liquid chromatography/mass spectrometry (LC/MS), fluorescence detection, enzyme-linked immuno sorbent assay (ELISA) [13–16]. For example, K Kuwayama *et al.* assessed the effectiveness of saliva and fingerprints as substitutes for urine and blood specimens, including convenience of sampling, sensitivity to drug testing, and duration of drug testing for each specimen type, and performed the analysis using LC/MS. Most analytes can be detected in saliva and fingerprints, as well as urine and blood. They have demonstrated that without using special technology or facilities, saliva and fingerprints can be easily collected on site [14]. G Hallvard *et al.* have studied the drug concentration ratio between oral fluid and blood for many chemicals, including benzodiazepines, opioids, carisoprodol, meprobamate and other chemicals by using HPLC. They determined the concentration ratio of 17 drugs in the oral fluid and blood, and used the concentration in the oral fluid to reliably estimate the concentration of the drug in the blood [13]. As can be seen from reports above, methods such as HPLC, LC/MS and ELISA are sensitive, accurate and reliable, however, they are also complicated, time-consuming, require professional personnel, and the instruments are usually very expensive, making them not suitable for long-term, frequent sample testing. Ideally, saliva detection can help patients with chronic disease to have frequent, painless tests, but only when economic and convenient detection tools are available at the same time.

Surface-enhanced Raman spectroscopy (SERS) has the potential to serve as a highly-sensitive, fast and convenient method for saliva drug testing. It is an optical imaging technique that features contact free, label-free, high-sensitivity and high-speed. Being fundamentally the same as Raman scattering, SERS detects inelastic scattering light, which contains information on specific molecular bond vibrations exist in the sample. Different detection limits were achieved under different situations [15,17–25]. Saiqa Muneer *et al*. proposed a target-specific nanomaterial using TNF-α functionalized gold-plated copper oxide chip to extract INF from human plasma and achieved a limit of detection (LOD) of 1.4 fM [15]. D Tu *et al*. fixed the DEHP aptamer on the magnetic particles, the silver nanoparticles were aggregated and coated with silica, and the silica particles were combined with the magnetic particles for measurement. Quantitatively determine the concentration of DEHP in the sample with an LOD of 8 pM [25]. G Shi *et al*. proposed a method for manufacturing Au nanoparticles/graphene oxide/cicada wing (Au NPs/GO/CW) substrates, and reached an LOD of 10^{-8} M [22].

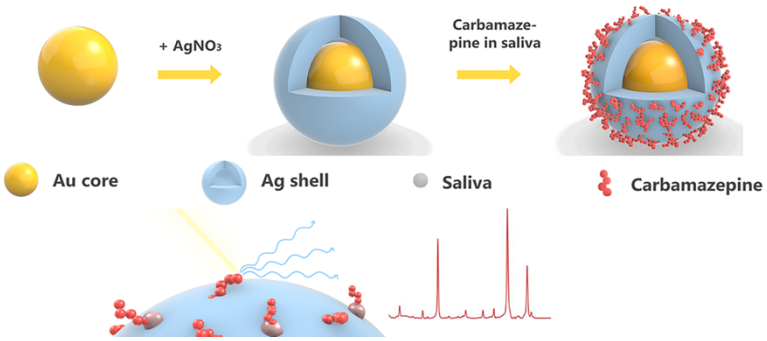

Fig. 1. The synthesis of Au@Ag NPs and the schematic diagram of the SERS detection of CBZ in saliva.

Biomedical Optics EXPRESS

In this study, we proposed a method of using SERS to non-invasively detect the CBZ in saliva (Fig. 1). Au-Ag core-shell nanomaterial substrates were prepared and optimized as SERS substrates. This method has reached a detection limit of 3.26×10^{-9} mol/L. It is one of the most sensitive methods reported for CBZ detection. This has introduced a potential method of using SERS to conveniently monitor the concentration of drugs in saliva as a painless alternative to blood testing.

2. Methods

2.1. Chemicals and reagents

Chloroauric acid tetrahydrate, sodium citrate dihydrate silver nitrate, methanol, and CBZ were purchased from MACKLIN (Shanghai, China). Deionized water of 18.25 MΩ was used in all following experiments.

2.2. Simulation, synthesis, optimization and characterization of Au@Ag NPs

The underlying mechanism of the hot spot-based Raman enhancing were demonstrated by the simulation of electromagnetic field distributions of the Au@Ag NPs aggregates with FDTD solutions [26]. Then aggregation states of Au@Ag NPs were stimulated with 1, 2, 3, 4 NPs.

The synthesis of the nanomaterials was performed in a Class 100 clean bench (SX-BHC, Su Xin, China). First, the Au NPs was prepared based on the reduction of $HAuCl_4$ solution with sodium citrate described by Frens G [27]. In brief, 2.5 mL of $HAuCl_4 \cdot 4H_2O$ (1wt%) solution was diluted and boiled in 250 mL deionized water with strong stirring. 2.5 mL of sodium citrate solution (1wt%) was rapidly added to the boiling mixture and continued to boil for 30 min. The heat was then turned off and the mixed solution was continuously stirred, as it cooled down to room temperature and stabilized. Au NPs were centrifuged at 9000 rpm for 20 min, then dispersed in 250 mL deionized water and stored at 4 °C for further use. Then Ag shell was then prepared. The 250 mL Au NPs was heated and stirred to 60 °C. Add a certain amount of sodium citrate (1wt%), then add 2.5 mL silver nitrate solution. After heating under stirring for 40 minutes, the solution was stirred continuously before cooled down to room temperature. Au@Ag NPs were obtained by centrifugation at 9000 rpm for 20 min, then kept at 4 °C for further use.

In the structure of Au@Ag NPs, silver ions in silver nitrate solution were reduced by sodium citrate, and the Ag NPs were coated on Au NPs. Therefore, the amount of silver ions involved in the reduction affects the thickness of the silver shell deposited on the gold core. To optimize SERS enhancement effect, 3 mL - 8 mL 1wt% sodium citrate solution was used to synthesize 6 substrates with different silver shell thickness. The amount of Au NPs remained unchanged, while the silver nitrate solution (0.1M) remained at 2.5 mL. The Au NPs and Au@Ag NPs were characterized by UV-3600 spectrometer (Shimadzu, Japan). The wavelength range of the UV-Vis absorption spectrometer was set to 300-800 nm, the spectral resolution was 1 nm, the integration time was 0.3s, and the scanning speed was 1200 nm/min [28]. In order to further determine the size and distribution of the prepared Au NPs and Au@Ag NPs, imaging was performed with a transmission electron microscope (TEM, FEI, Hillsborough, or the United States), and dynamic light scattering measurements (Zetasizer, Nano-ZS90, Mohr Wen, UK) were performed.

2.3. Simulation and Raman measurements of CBZ powder sample

The expected Raman spectrum of CBZ was simulated. The chemical formula of CBZ was input into Chem 3D for modeling. It was used to generate 3D models of CBZ molecule, which was then input into GaussView, where parameters such as the distance and angle between atoms were optimized. Then the data from GaussView was imported into Gaussian to acquire the simulated Raman spectrum based on the density function theory (DFT) [29].

Biomedical Optics EXPRESS

The experimental Raman spectra of solid CBZ was acquired by placing a small amount of CBZ powder (Aladdin Reagent, Shanghai China) on the glass slide and image with microscopic Raman spectrometer (LabRAM Xplora Plus, HORIBA Scientific, France). Raman spectra ranging from 300 to 1800cm^{-1} were recorded with an incident laser wavelength of 638 nm and a 10 × objective lens. The typical accumulation time used in this study was 2s [30,31].

2.4. Preparation and SERS measurements of standard CBZ solution

Standard CBZ solution was prepared by adding CBZ powder in methanol (Aladdin Reagent, Shanghai, China) and deionized water (methanol/deionized water=1:1, v/v). By adjusting the pH of CBZ solution with hydrochloric acid, the SERS properties under different pH conditions were compared, and the best conditions were selected according to the optimal SERS results.

A series of CBZ solutions with eight concentrations (1×10^{-1} to 1×10^{-8} mol/L) were prepared. Au@Ag NPs were used as SERS enhancing substrate to collect the spectra of CBZ solutions with different concentrations. Generally, 50 µL Au@Ag NPs solution and 40 µL CBZ solution with a certain concentration were mixed for 1 h to obtain a stable solution. 5 µL mixture was placed on a glass slide for SERS measurement with the Raman microscope described in section 2.3. For each sample, the SERS spectra of 10 random positions were measured and an average spectrum was obtained.

2.5. Preparation and SERS measurements of CBZ saliva solution

CBZ in saliva was used as mimic of real samples. In this experiment, saliva was collected from healthy and drug-free volunteers. 10 mL of saliva was collected and was first diluted with phosphate buffer (saliva, 1:10 dilution). Then different concentrations of CBZ were added to achieve a series of concentrations (1×10^{-1} to 1×10^{-8} mol/L). Then shake the centrifuge tube for 30s and mix evenly. According to the method described in section 2.4, the mixed Au@Ag NPs solution and CBZ saliva solution were obtained and adjusted to the optimum pH. Each sample was allowed to equilibrate at room temperature for 30 minutes before SERS experiment. SERS spectra were acquired with the instrument described in section 2.3. Ten repeated measurements were made for each sample. In order to eliminate the interference of background solution, SERS spectra of pH optimized saliva solution without CBZ were also collected.

2.6. Spectral data processing

Preprocessing including noise reduction and baseline correction was performed in labspec6 to optimize the Raman and SERS spectra [32]. Then, correlation between the characteristic peak intensity of the SERS spectrum and the solution concentration was analyzed, and the linear relationship between the characteristic peak intensity of CBZ and the logarithm of the CBZ concentration in the sample was established. When the concentration range is large, the linear relationship between the peak intensity and the logarithmic concentration is usually adopted [33]. Ten repeated measurements were used to provide the average intensity and the standard deviation when establishing the linear equation for quantitative evaluation, and R^2 was used to evaluate the linearity. Relative standard deviation (RSD) was also calculated to acquire the precision of measurements [34–36]. Limit of detection (LOD) was calculated based on the definition, three times the value of the instrument background signal generated by the matrix blank (S/N = 3), as described in literatures [37].

2.7. SERS repeatability and longitudinal measurements

To verify the repeatability of the proposed method, SERS mapping images were acquired with 10^{-4} mol/L CBZ solution and Au@Ag NPs mixed at a volume of 1:1. Specifically, a 60 × 60 µm^2 area (12 × 12 pixels) were mapped and 144 spectra were recorded and analyzed. To verify the durability of the enhanced effects of Au@Ag NPs, the SERS spectra of CBZ solution at

Biomedical Optics EXPRESS

concentrations of 10^{-4} mol/L were measured every seven days. The enhancement effect was evaluated through 35 days.

3. Results and discussion

3.1. Optimization and characterization of Au@Ag NPs

The thickness of Ag shell was optimized by using different amount of sodium citrate to reduce silver nitrate. SERS spectra were obtained for each substrate. As can be seen in Fig. 2, among the substrates made with 3 mL - 8 mL sodium citrate, 6 mL sodium citrate had the best SERS enhancement effect. This was reasonable because when a larger amount of silver nitrate solution was reduced with increasing sodium citrate, more Ag NPs were generated to be attached to the surface of Au NPs and form a thicker shell structure on the Au core, resulting in increased surface plasmon resonance activity and thus more hotspots [38–41]. When the NPs are too small, the effective conductivity and light scattering characteristics required for SERS enhancement will decrease and the quality of surface plasmon resonance activity will be deteriorated [42]. With the increase of particle sizes, surface plasmon resonance activity increases [43]. However, when the size of particles increases to the scale of excitation wavelength, the particles would be preferentially excited in the non-radiation mode, leading to the weakening of SERS effect [42,44]. Some reported that the optimum size of enhancing particles was 30 nm ~ 100 nm [45]. The case of using 6 mL sodium citrate solution presented the highest SERS enhancement effect. As can be seen from Fig. 3, the average diameter of Au@Ag NPs was 45 nm, which was in the optimum range in previous reports. This substrate was used in all experiments and analysis in this study.

The Au and Au@Ag NPs were characterized with UV-Vis spectrometer, TEM and dynamic light scattering. As indicated in Fig. 3(a), an obvious absorption peak at 520 nm was present in the UV-Vis spectrum. The location of the peak matched the surface plasmon resonance of Au NPs. With increased silver shell thickness, the absorption peak blue-shifted to 400 nm, due to the increase in particle volume and the dielectric properties of silver [46]. This also verified the core-shell structure of Au@Ag core-shell nanostructures. Figure 3(b, c) showed that the Au NPs were spherical and monodispersed with a size approximately 25 nm. Au@Ag NPs were monodispersing, approximately spherical in shape, with an average diameter of 45 nm.

Through FDTD, the electromagnetic field distribution of Au@Ag NP aggregates was simulated to explain the mechanism of hot spot-based Raman signal enhancement. According to Fig. 4, statistical result of interparticle distance between the Au@Ag NPs was mostly 5 nm. The possible aggregation state of particles was simulated. Compared with a single particle, there were hot spots among multiple particles, and aggregates exhibited stronger electromagnetic effects. The experimental data was consistent with the FDTD result, which provided the theoretical basis for the method.

3.2. CBZ spectrum simulation and characteristic peak assignments

The DFT simulated spectrum, Raman spectrum of CBZ powder and the SERS spectrum of CBZ solution were shown in Fig. 5. The agreement between DFT simulated spectrum and CBZ solid powder spectrum was remarkable. All the principal Raman peaks in the experimental spectrum corresponded to a counterpart in the DFT simulated spectrum. SERS also had good correspondence with the Raman spectrum and DFT simulation results, although SERS presented fewer peaks, which was quite common. As shown in Fig. 5, SERS measurements of CBZ showed characteristic peaks at 398 cm^{-1}, 611 cm^{-1}, 754 cm^{-1}, 1011 cm^{-1}, 1173 cm^{-1}, 1272 cm^{-1}, 1400 cm^{-1}, and 1582 cm^{-1}, which were also consistent with previously reported results. The peak at 398 cm^{-1} was assigned to the skeletal vibrations δ(C-C); the peak at 611 cm^{-1} was coupled to the δ(C-N) vibration; the peak at 754 cm^{-1} originated from the δ(C-H) stretching peaks; the peaks at 1011 cm^{-1} and 1173 cm^{-1} resulted from the ν(C-C); the peak at 1272 cm^{-1} corresponded to

Biomedical Optics EXPRESS

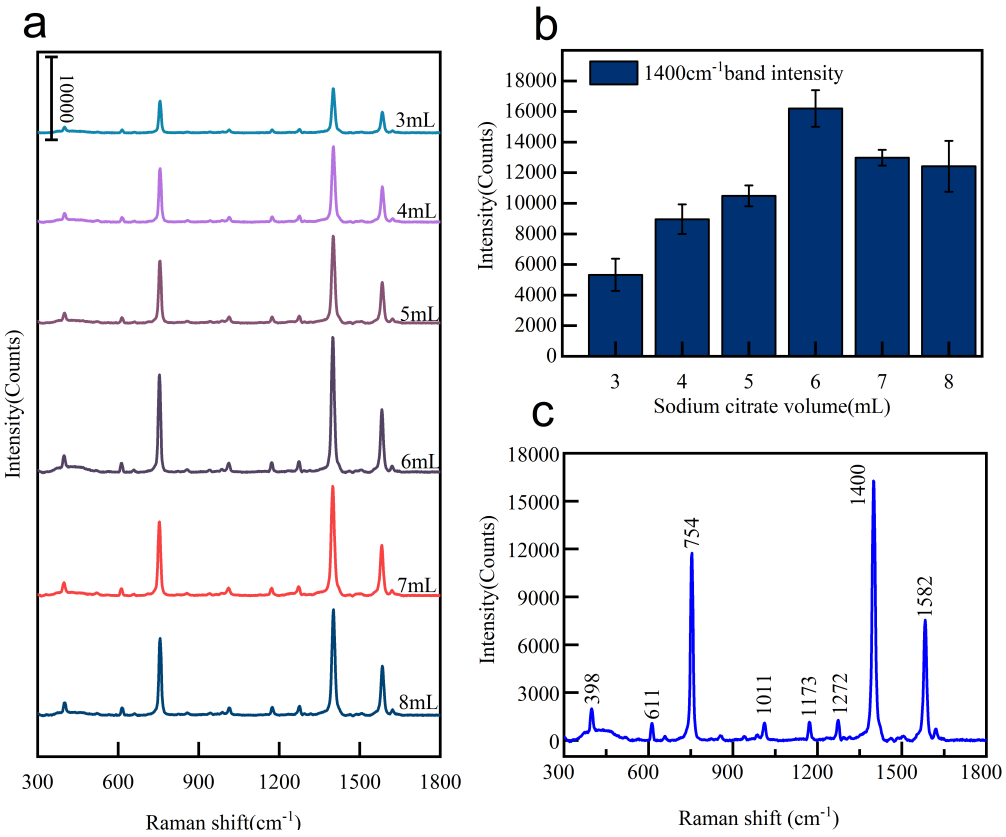

Fig. 2. (a) SERS spectra of CBZ solution of 10^{-4} mol/L using Au@Ag substrates made with 3 - 8 mL sodium citrate. (b) SERS intensity bar graph at 1400 cm^{-1}. (c) SERS spectra of 10^{-4} mol/L CBZ solution with Au@Ag NPs synthesized with 6 mL sodium citrate. The error bar represented the standard deviation from five measurements.

the τ(NH2) stretching band; the peak at 1400 cm^{-1} originated from the ν(C-N) stretching bands; the peak at 1582 cm^{-1} originated from the δ(NH2) stretching bands. Both Raman and SERS measurements presented peak shifts. As frequently reported, there can be obvious shifts between SERS and Raman peaks, due to the chemical interactions between sample and the enhancing substrate used in the experiment [47,48]. The spectra and their peak assignments were indicated in Fig. 5 and Table 1.

3.3. SERS measurements and analysis of standard CBZ solution

3.3.1. Optimization of pH

Under different pH conditions, the amount of hot spots produced by the combination of the substrate and the drug was different. Therefore, changing the content of hydrochloric acid in CBZ solution to adjust pH can optimize enhancement effect. The enhancement effect of pH = 1 - 10 was measured with 10^{-4} mol/L CBZ standard solution. The SERS spectra of 10^{-4} mol/L CBZ standard solution under pH=1, 2 and 3 were presented in Fig. 6. When pH = 4 - 10, no signal was detected. It can be clearly observed that the SERS activity was the strongest with pH = 2.

Biomedical Optics EXPRESS

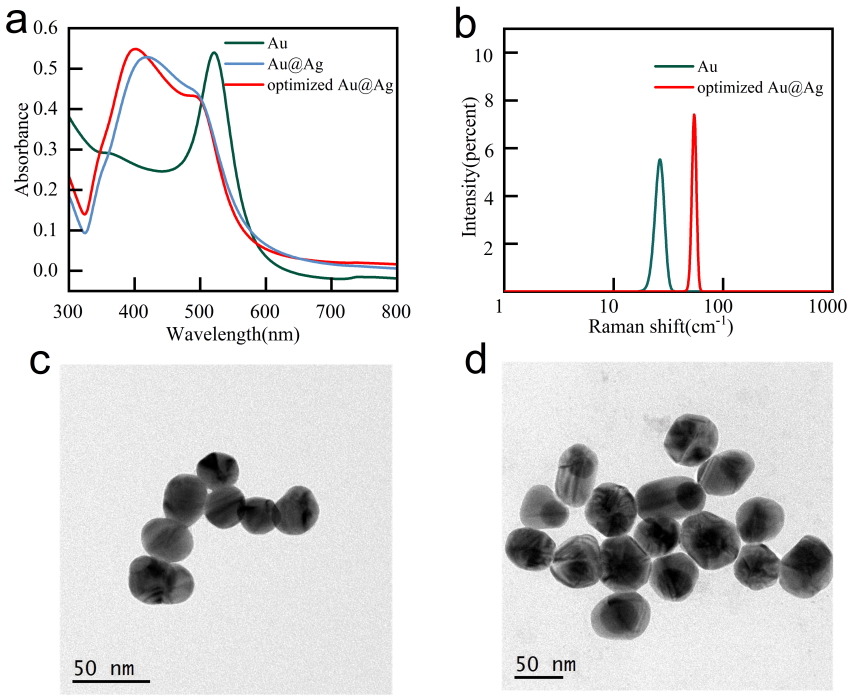

Fig. 3. (a) The UV-Vis spectra of Au NPs, the Au@Ag NPs prepared with 4 mL 1 wt% sodium citrate and the optimized Au@Ag NPs prepared with 6 mL 1 wt% sodium citrate. (b) The particle size distribution of the Au NPs and the optimized Au@Ag NPs. (c) TEM image of Au NPs. (d) TEM image of optimized Au@Ag NPs.

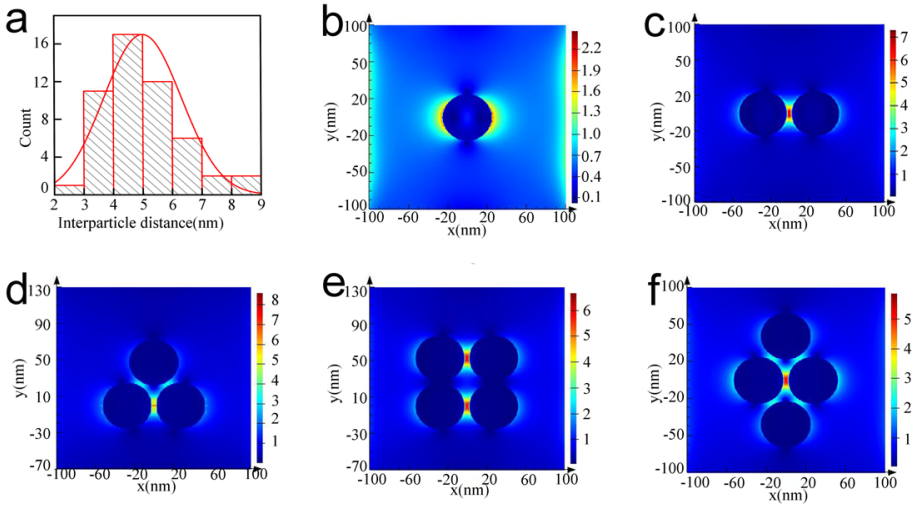

Fig. 4. (a) Statistical results of interparticle distance of Au@Ag NPs. (b – f) The electric field distribution of Au@Ag NPs is simulated by FDTD method.

Biomedical Optics EXPRESS

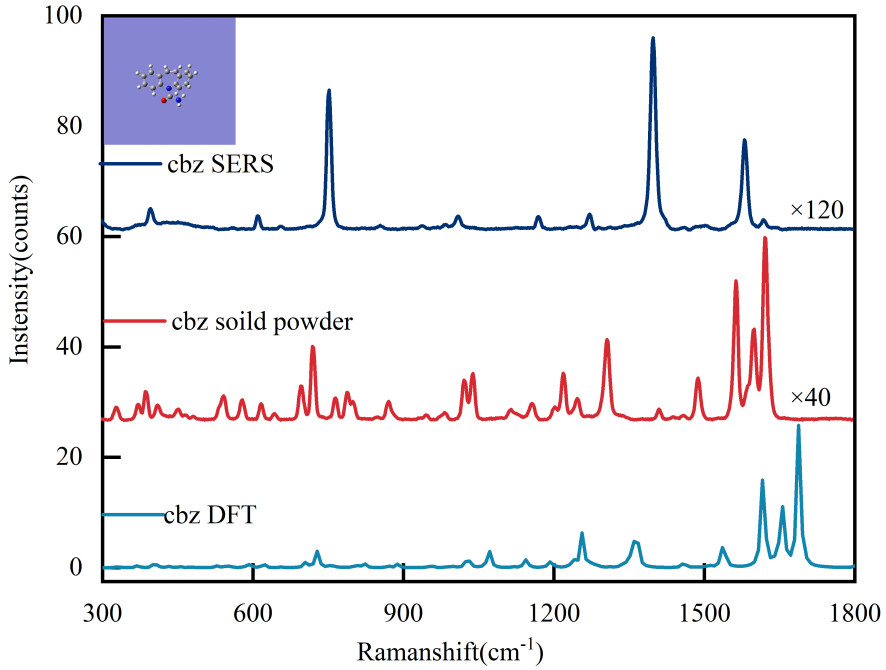

Fig. 5. SERS spectra of 10^{-4} mol/L CBZ solution in the presence of Au@Ag NPs, Raman spectrum of CBZ in solid state, and CBZ DFT simulated spectrum (average from six measurements).

Table 1. Assignments of DFT, Raman and SERS spectral peaks of 10^{-4} mol/L CBZ

CBZ with DFT (cm^{-1})	CBZ solid sample (cm^{-1})	CBZ with Au@Ag NPs enhanced SERS (cm^{-1})	Assignment
400	388	398	δ(C-C)
592	619	611	δ(C-N)
728	721	754	δ(C-H)
1024	1023	1011	ν(C-C)
1144	1157	1173	ν(C-C)
1256	1249	1272	τ(NH2)
1450	1412	1400	ν(C-N)
1656	1600	1582	δ(NH2)

3.3.2. Au and Au@Ag substrates comparison

Au NPs themselves presented SERS enhancement effect and was a common substrate used in SERS experiments. The enhancement effect of optimized Au@Ag NPs was compared to that of the Au NPs, and it was found that Au@Ag NPs provided much better enhancement in the detection of CBZ. As shown in the Fig. 7, the optimized Au@Ag NPs provided SERS signals much stronger than Au NPs or Raman signals of CBZ powder. The SERS intensity of the band at 1400 cm^{-1} was 25 times stronger than that of powder CBZ and was 10 times higher than that that with the Au NP substrate. The Au@Ag NPs were able to combine the advantage of Au NPs and Ag NPs. Ag has stronger enhancement effect while Au NPs has good stability [49]. Therefore,

Biomedical Optics EXPRESS

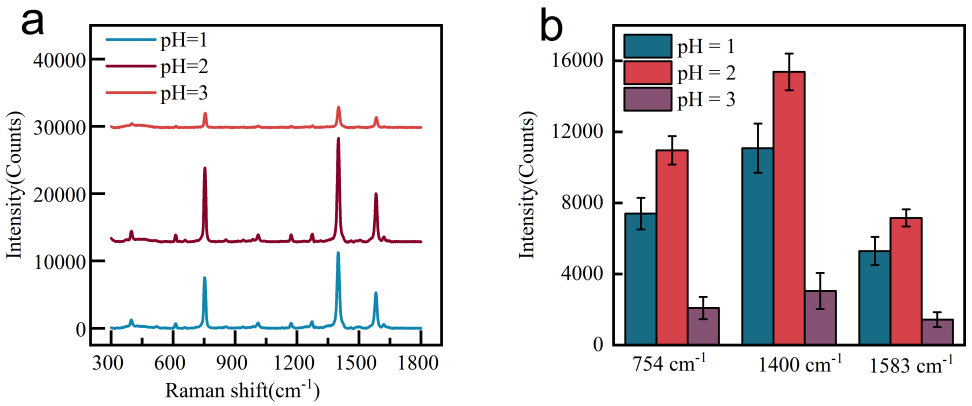

Fig. 6. (a) The average SERS spectra of 10^{-4} mol / L CBZ solution at pH = 1, 2, 3. (b) SERS intensity of characteristic peaks at 754 cm^{-1} 1400 cm^{-1} 1583 cm^{-1} under pH = 1, 2, 3 respectively. Error bars indicated the standard deviations from ten measurements.

based on these advantages, using optimized Au@Ag NPs can provide better enhancement effect than Au NPs alone.

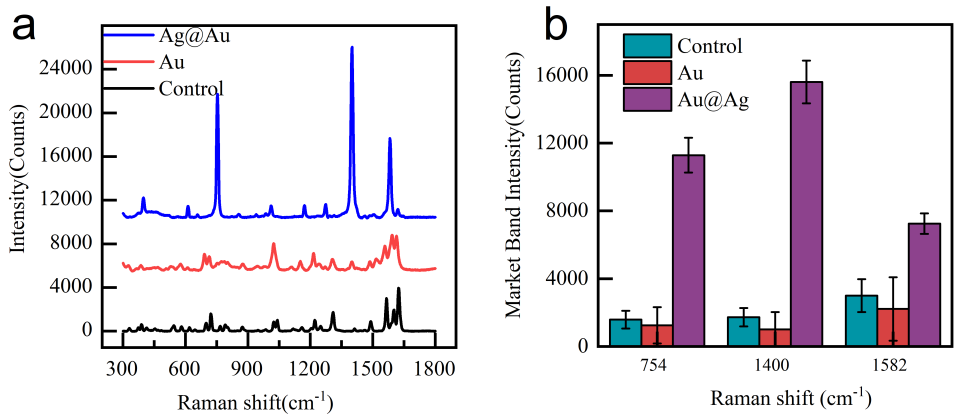

Fig. 7. (a) SERS spectra of 10^{-4} mol/L CBZ solution with Au@Ag NPs, Au NPs, and Raman spectrum of CBZ in solid state as control. (b) SERS intensity of characteristic bands 754 cm^{-1}, 1400 cm^{-1}, and 1582 cm^{-1} of solid CBZ as control, CBZ solution with Au NPs, and CBZ solution with Au@Ag NPs, respectively.

3.3.3. SERS measurements and analysis of standard CBZ solution with Au@Ag NPs

Eight different concentrations of CBZ standard solution were measured with SERS. The signals showed a decreasing trend as the concentration decreases (Fig. 8). Table 2 showed the linear equations between logarithm intensity and the concentration at three characteristic peaks. R^2 values ranged from 0.9663 to 0.9753, with the characteristic peak at 1400 cm^{-1} being the most prominent. The relationship between the intensity of characteristic peak 1400 cm^{-1} and CBZ concentration was shown in Fig. 9. The calculated theoretical detection limit was 1.26×10^{-9} mol/L.

Biomedical Optics EXPRESS

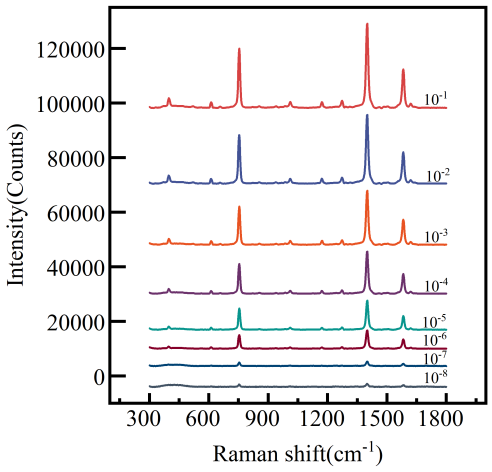

Fig. 8. SERS spectra of the CBZ standard solution of eight concentrations (10^{-1} to 10^{-8} mol/L) averaged from 10 measurements.

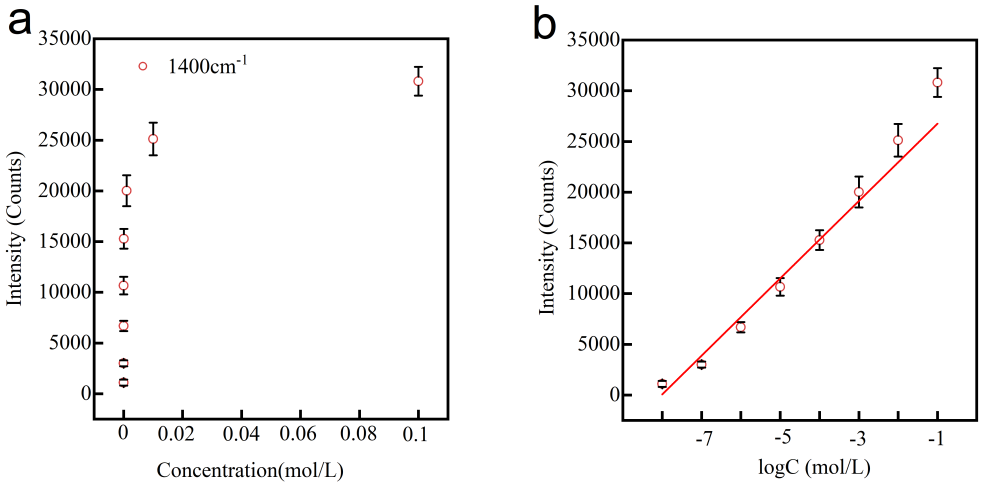

Fig. 9. The linear relationship established for the CBZ standard solutions. The relationship between the intensity of the SERS characteristic peak at 1400 cm^{-1} and the concentration of CBZ shown in linear coordinates (a) and (b) logarithmic coordinates.

Table 2. Linear regression of Raman intensity for each marker band ($\Delta v = 754\ cm^{-1}$, $1400\ cm^{-1}$, $1582\ cm^{-1}$) in the concentration ranging from 1×10^{-8} to 1×10^{-1} mol/L

Raman shift (cm^{-1})	Equation	LOD (mol/L)	R^2
754	y = 21282.8820 + 2618.0246x	6.31×10^{-9}	0.9663
1400	y = 31083.2286 + 3917.2316x	1.26×10^{-9}	0.9753
1582	y = 14399.7024 + 1793.8496x	7.59×10^{-9}	0.9728

Biomedical Optics EXPRESS

3.4. SERS measurements and analysis of CBZ saliva solution

The background of saliva solution was first characterized with SERS. As shown in Fig. 10, the characteristic peak of hydrochloric acid was observed at 412 cm^{-1} in the pH optimized saliva solution. The peak came from hydrochloric acid, and the intensity was small, so it had no effect on the SERS spectrum of CBZ. The detection of CBZ in saliva was used at mimic of real samples. SERS spectra of CBZ in saliva were shown in Fig. 11. The SERS characteristic peaks at 398 cm^{-1}, 611 cm^{-1}, 754 cm^{-1}, 1011 cm^{-1}, 1173 cm^{-1}, 1272 cm^{-1}, 1400 cm^{-1}, and 1582 cm^{-1} were clearly observed in all spectra. The characteristic peaks of CBZ measured in saliva were in excellent agreement with the CBZ standard solution. In Table 3, the linear equations between logarithm intensity and CBZ concentrations were established at the three characteristic peaks. By comparing R^2 values, the linearity at 1400 cm^{-1} was the most prominent at all three characteristic peaks. The linear relationship between the intensity of the characteristic peak at 1400 cm^{-1} and the concentration of the sample solution was shown in Fig. 12(b). The results were consistent with the measurements of CBZ standard solution, and it showed that the quantitative determination of CBZ in saliva was feasible. The calculated detection limit (LOD) was 3.26×10^{-9} mol/L(S/N=3). The reported effective therapeutic plasma concentration range of CBZ was 4 ~ 12 μg/mL, corresponded to the concentration range of CBZ in saliva from 4.2×10^{-6} to 1.25×10^{-5} mol/L, which was within the detection range of the experiment. The measured range (10^{-1} to 10^{-8} mol/L) covered the effective range of CBZ and was able to provide several orders of magnitudes measurements outside this range.

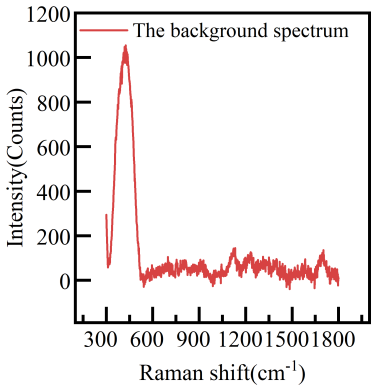

Fig. 10. SERS spectrum of a mixed solution of saliva and hydrochloric acid

Table 3. Linear regression of Raman intensity for each marker bands ($\Delta\nu$ = 754 cm^{-1}, 1400 cm^{-1}, 1582 cm^{-1}) in the concentration ranging from 1×10^{-8} to 1×10^{-1} mol/L

Raman shift (cm^{-1})	Equation	LOD (mol/L)	R^2
754	y = 21282.8820 + 2618.0246x	8.31×10^{-9}	0.9463
1400	y = 31083.2286 + 4255.2539x	3.26×10^{-9}	0.9541
1582	y = 14399.7024 + 1793.8496x	9.59×10^{-9}	0.9328

In order to confirm the accuracy of the SERS measurements, we calculated the relative standard deviation (RSD) of the concentration gradient between the CBZ standard solution and the sample solution, as shown in Table 4. In the CBZ standard solution and sample solution, the RSD value gradually increased as the concentration of the solution decreased, but they were still under

Biomedical Optics EXPRESS

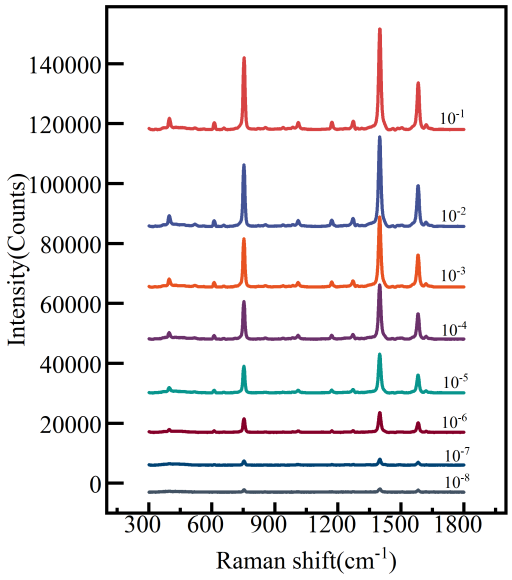

Fig. 11. SERS spectra of saliva samples treated with eight concentrations of CBZ (10^{-1} to 10^{-8} mol/L), averaged from 10 repeated measurements.

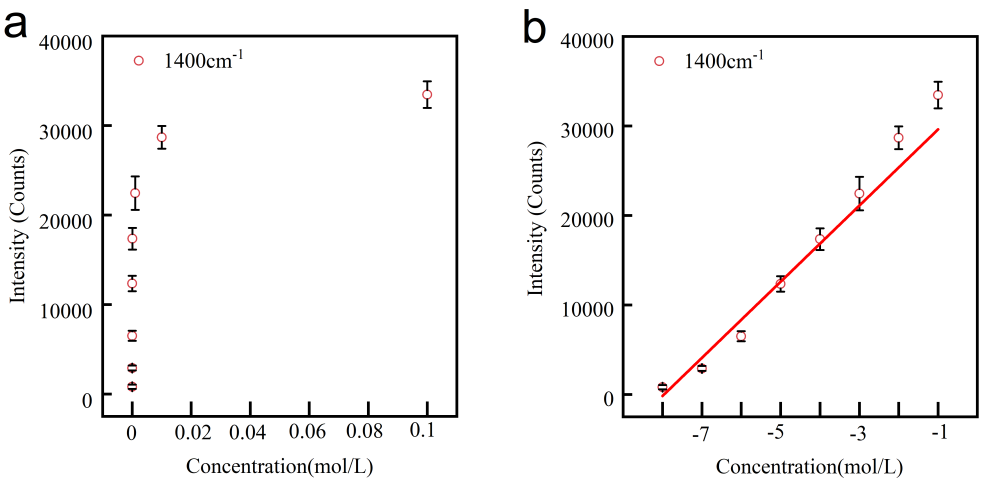

Fig. 12. The linear relationship established for the CBZ saliva solutions. The relationship between the intensity of the SERS characteristic peak at 1400 cm^{-1} and the concentration of CBZ shown in linear coordinates (a) and logarithmic coordinates (b).

Biomedical Optics EXPRESS

10%, which was considered reasonable in SERS measurement [34]. It showed that the Au@Ag substrates can be used for CBZ detection, with high sensitivity and sufficient accuracy.

Table 4. Standard deviation calculation result of standard solution and sample solution

	Concentrations (mol/L)	10^{-1}	10^{-2}	10^{-3}	10^{-4}	10^{-5}	10^{-6}	10^{-7}	10^{-8}
Standard solution	RSD (%)	2.6	3.4	3.6	4.4	5.2	6.5	7.3	8.6
Sample solution	RSD (%)	2.4	3.4	3.9	4.7	6.1	7.6	8.5	8.9

The detection limit using the proposed method was similar to previous studies using different techniques. L Budakova *et al*. used HPLC to detect CBZ in methanol solution, and the detection limit reached 2.1×10^{-6} mol/L [50]. X. S Miao *et al*. used liquid chromatography-electrospray tandem mass spectrometry to measure CBZ and its metabolites in water samples, and the detection limit was 1.27×10^{-7} mol/L [51]. A.M Tsatsakis *et al*. used immunoassay and gas chromatography to detect CBZ in hair, the detection line is 8.8×10^{-9} mol/L [52]. J Hermida *et al*. used whole-body immunoassay and high performance liquid chromatography to measure the concentration of CBZ in the plasma of epilepsy patients with a detection limit of 1.05×10^{-8} mol/L [53]. Although the instruments used in these studies could reach much lower detection limits, it was usually not necessary to detect CBZ at a much lower concentration. The range of CBZ concentration measured in our study was consistent with previous reports regarding the need for CBZ detection. Standard detection methods such as HPLC, etc. are sensitive, accurate, and reliable, but they also have problems such as complex, expensive, time-consuming, and require professionals. In contrast, SERS has the advantages of fast, non-contact, label-free, and economic, etc., which made it an ideal alternative for on-site detection.

3.5. SERS repeatability and longitudinal measurements

An important application for this method was to use it in clinics, therefore the repeatability was extremely important. Figure 13 showed 121 repeated SERS measurements from a 60 by 60 μm area on a 10^{-4} mol/L CBZ solution sample. In the presence of Au@Ag NPs, the intensity bar graph of the SERS spectrum of the CBZ sample at 1400 cm^{-1} and the SERS mapping image detection of the 1400 cm^{-1} peak show that the enhancement effect was uniform.

The longitudinal measurement results were shown in Fig. 14. The enhancement effect of the Au@Ag NPs gradually weakened with the increase of time, but the enhancement effect of the

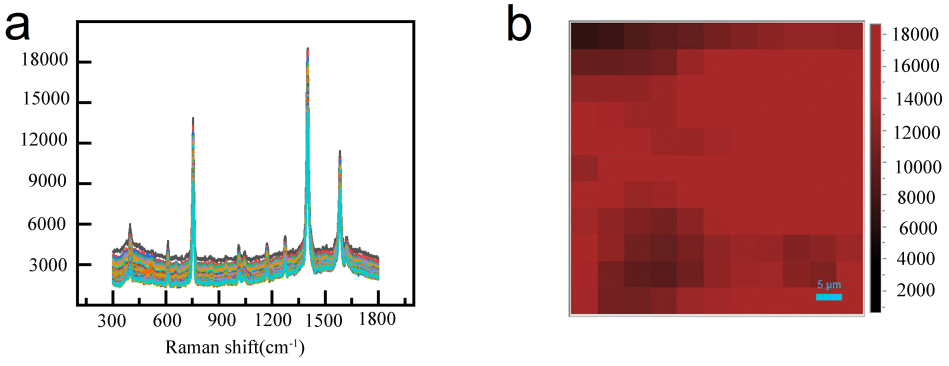

Fig. 13. (a) SERS spectra of 121 different points treated with 10^{-4} mol/L CBZ saliva sample solution. (b) The SERS mapping image at 1400 cm^{-1}.

Biomedical Optics EXPRESS

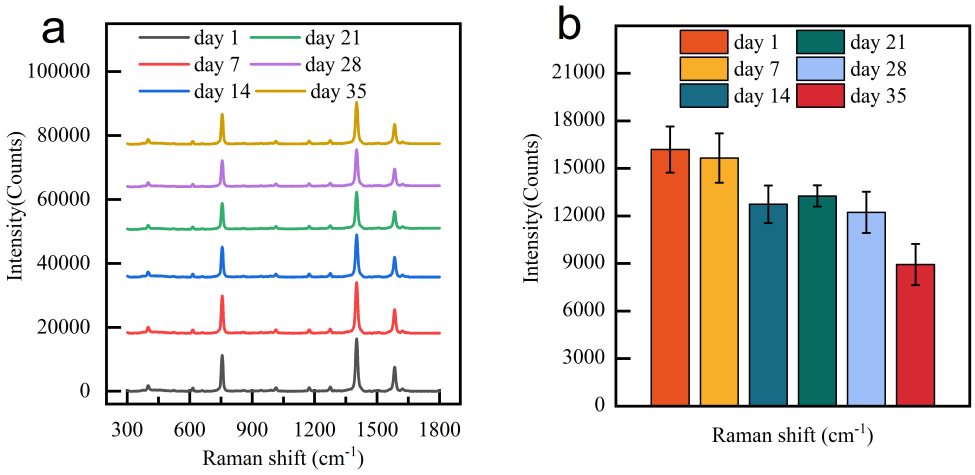

Fig. 14. (a) SERS spectra of 10^{-4} mol/L CBZ solution taken every 7 days. (b) The peak intensity of at 1400 cm^{-1} shown in bar graph.

substrate was generally satisfactory throughout 35 days. This demonstrated the stability of the enhancement effect of the substrate over time.

4. Conclusion

In this work, a contact-free, label-free, and highly-sensitive salivary CBZ monitoring strategy based on Au@Ag composite material was proposed. This combination of strong electromagnetic enhancement with Au-Ag core-shell nanomaterials and good biocompatibility showed remarkable ability to help the detection of molecules in a bioenvironment. Through the optimization of the Au@Ag NPs, a large number of SERS hot spots were produced, and greatly improved the Raman signal of the target CBZ molecule. It was shown that this method had a detection limit of 3.26×10^{-9} mol/L for CBZ in saliva, with a linear detection range from 1×10^{-8} mol/L to 1×10^{-1} mol/L, which was more than adequate for CBZ detection in the saliva. The spectra showed excellent correspondence between the theoretical spectrum and experimental results, demonstrating high accuracy at very low concentrations.

Most importantly, compared with traditional assays such as HPLC, LC-MS/MS and ELISA, this strategy has the advantages of convenience and low-cost, and has great potential for CBZ monitoring in saliva as an alternative to frequent blood tests. In addition, Au@Ag NPs, with their reliable performance and good biocompatibility, can serve in many advanced applications in the fields of medicine and biotechnology.

Funding. National Key Research and Development Program of China (No. 2017YFC0110200); National Natural Science Foundation of China (No. 61805143); Shanghai Sailing Program (No. 18YF1409500).

Disclosures. The authors declare that there are no conflicts of interest related to this article.

Data availability. Data underlying the results presented in this paper are not publicly available at this time but may be obtained from the authors upon reasonable request.

References

1. R. H. Mattson, J. A. Cramer, and J. F. Collins, "A Comparison of Valproate with Carbamazepine for the Treatment of Complex Partial Seizures and Secondarily Generalized Tonic–Clonic Seizures in Adults," N. Engl. J. Med. **327**(11), 765–771 (1992).
2. H. Wei and P. J. Vikesland, "pH-Triggered Molecular Alignment for Reproducible SERS Detection via an AuNP/Nanocellulose Platform," Sci. Rep. **5**(1), 18131 (2015).

Biomedical Optics EXPRESS

3. A. J. Heller, P. Chesterman, R. D. Elwes, and P. Crawford, "Phenobarbitone, phenytoin, carbamazepine, or sodium valproate for newly diagnosed adult epilepsy: a randomised comparative monotherapy trial," J. Neurol., Neurosurg. Psychiatry **58**(1), 44–50 (1995).
4. A. G. Berger, S. M. Restaino, and I. M. White, "Vertical-flow paper SERS system for therapeutic drug monitoring of flucytosine in serum," Anal. Chim. Acta **949**(1), 59–66 (2017).
5. C. Shende, C. Brouillette, and S. Farquharson, "Detection of codeine and fentanyl in saliva, blood plasma and whole blood in 5-minutes using a SERS flow-separation strip," Analyst **144**(18), 5449–5454 (2019).
6. M. Teunissen, M. Torren, N. Vermeulen, and D. D. Breimer, "Automated HPLC-determination of antipyrine and its main metabolites in plasma, saliva and urine, including 4,4′-dihydroxyantipyrine," J. Chromatogr. A **278**(2), 367–378 (1984).
7. T. Yang, X. Guo, H. Wang, and S. Fu, "Magnetically optimized SERS assay for rapid detection of trace drug-related biomarkers in saliva and fingerprints," Biosens. Bioelectron. **68**, 350–357 (2015).
8. K. W. Stephen, J. Mccrossan, D. Mackenzie, C. B. Macfarlane, and C. F. Speirs, "Factors determining the passage of drugs from blood into saliva," Br. J. Clin. Pharmacol. **9**(1), 51–55 (1980).
9. K. Langel, H. Gjerde, D. Favretto, and P. Lillsunde, "Comparison of drug concentrations between whole blood and oral fluid," Drug Test. Analysis **6**(5), 461–471 (2013).
10. D. Lee and M. A. Huestis, "Current knowledge on cannabinoids in oral fluid," Drug Test. Anal. **6**(1-2), 88–111 (2014).
11. V. Vindenes, B. Yttredal, E. Liestad, and H. WaalJ, "Oral Fluid is a Viable Alternative for Monitoring Drug Abuse: Detection of Drugs in Oral Fluid by Liquid Chromatography-Tandem Mass Spectrometry and Comparison to the Results from Urine Samples from Patients Treated with Methadone or Buprenorphine," J. Anal. Toxicol. **35**(1), 32–39 (2011).
12. S. Pynnonen, "The pharmacokinetics of carbamazepine in plasma and saliva of man," Basic Clin. Pharmacol. Toxicol. **41**(5), 465–471 (2009).
13. H. Gjerde, J. Mordal, and A. S. Christophersen, "Comparison of drug concentrations in blood and oral fluid collected with the Intercept sampling device," J. Anal. Toxicol. **34**(4), 204–209 (2010).
14. K. Kuwayama, H. Miyaguchi, T. Yamamuro, K. Tsujikawa, and H. Inoue, "Effectiveness of saliva and fingerprints as alternative specimens to urine and blood in forensic drug testing," Drug Test. Analysis **8**(7), 644–651 (2016).
15. M. Saiqa, A. A. Godwin, N. Islam, and L. I. Emad, "Preconcentration and SERS-based determination of infliximab in blood by using?a TNF-α-modified gold-coated copper oxide nanomaterial," Microchim. Acta **186**(12), 780 (2019).
16. S. W. Toennes, S. Stefan, and H. Maurer, "Screening for drugs of abuse in oral fluid–correlation of analysis results with serum in forensic cases," J. Anal. Toxicol. **29**(1), 22–27 (2005).
17. O. J. Achadu, F. Abe, and T. Suzuki, "Molybdenum Trioxide Nanocubes Aligned on a Graphene Oxide Substrate for the Detection of Norovirus by Surface-Enhanced Raman Scattering," ACS Appl. Mater. Interfaces **12**(39), 43522–43534 (2020).
18. Y. Du, H. Liu, Y. Tian, C. Gu, Z. Zhao, S. Zeng, and T. Jiang, "Recyclable SERS-Based Immunoassay Guided by Photocatalytic Performance of Fe3O4@TiO2@Au Nanocomposites," Biosensors **10**(3), 25 (2020).
19. P. Liang, Y. Cao, Q. Dong, and C. Wang, "A balsam pear-shaped CuO SERS substrate with highly chemical enhancement for pesticide residue detection," Microchim. Acta **187**(6), 335 (2020).
20. S. Muneer, G. A. Ayoko, and N. Islam, "Utilizing the thiol chemistry of biomolecules for the rapid determination of anti-TNF-α drug in blood," Talanta **208**(1), 120411 (2020).
21. X. H. Pham, E. Hahm, T. H. Kim, H. M. Kim, and B. H. Jun, "Enzyme-amplified SERS immunoassay with Ag-Au bimetallic SERS hot spots," Nano Res. **13**(12), 3338–3346 (2020).
22. G. Shi, M. Wang, Y. Zhu, and L. Shen, "A flexible and stable surface-enhanced Raman scattering (SERS) substrate based on Au nanoparticles/Graphene oxide/Cicada wing array," Opt. Commun. **412**(1), 28–36 (2018).
23. S. Fujii, T. Maeda, I. Noge, and Y. Kitagawa, "Determination of acetone in saliva by reversed-phase liquid chromatography with fluorescence detection and the monitoring of diabetes mellitus patients with ketoacidosis," Clin. Chim. Acta **430**(1), 140–144 (2014).
24. D. Song, R. Yang, and C. Wang, "Reusable nanosilver-coated magnetic particles for ultrasensitive SERS-based detection of malachite green in water samples," Sci. Rep. **6**(1), 22870 (2016).
25. D. Tu, J. T. Garza, and C. GerardL, "A SERS aptasensor for sensitive and selective detection of bis(2-ethylhexyl)phthalate," RSC Adv. **9**(5), 2618–2625 (2019).
26. L. I. Li-Mei, P. P. Fang, Z. L. Yang, and W. D. Huang, "Size Dependent SERS Activity of Gold Nanoparticles Studied by 3D-FDTD Simulation," Spectroscopy & Spectral Analysis **29**(5), 1222–1230 (2009).
27. G. Frens, "Controlled Nucleation for the Regulation of the Particle Size in Monodisperse Gold Suspensions," Nat. Phys. Sci. **241**(105), 20–22 (1973).
28. G. Park, C. Lee, D. Seo, and H. Song, "Full-color tuning of surface plasmon resonance by compositional variation of Au@Ag core-shell nanocubes with sulfides," Langmuir **28**(24), 9003–9009 (2012).
29. W. M. Berhanu, I. A. Mikhailov, and A. E. Masunov, "Are density functional theory predictions of the Raman spectra accurate enough to distinguish conformational transitions during amyloid formation?" J. Mol. Model **16**(6), 1093–1101 (2010).
30. J. L. Yang, J. Xu, H. Ren, and L. Sun, "In situ SERS study of surface plasmon resonance enhanced photocatalytic reactions using bifunctional Au@CdS core–shell nanocomposites," Nanoscale **9**(1), 19–24 (2017).

Biomedical Optics EXPRESS

31. M. Tahir, B. Tahir, N. Amin, and Z. Y. Zakaria, "Photo-induced reduction of CO2 to CO with hydrogen over plasmonic Ag-NPs/TiO2 NWs core/shell hetero-junction under UV and visible light," J. Co2 Util. J Co2 Util. **18**, 250–260 (2017).
32. C. Lofrumento, M. Ricci, E. Platania, M. Becucci, and E. Castellucci, "SERS detection of red organic dyes in Ag-agar gel," J. Raman Spectrosc. **44**(1), 47–54 (2013).
33. Z. Wu, D. He, and B. Cui, "Trimer-based aptasensor for simultaneous determination of multiple mycotoxins using SERS and fluorimetry," Microchim. Acta **187**(9), 495 (2020).
34. K. Wu, T. Rindzevicius, and M. S. Schmidt, "Optimizing silver-capped silicon nanopillars to simultaneously realize macroscopic, practical-evel SERS signal reproducibility and high enhancement at low costs," J. Raman Spectrosc. **48**(12), 1808–1818 (2017).
35. G. Xiao, Y. Li, W. Shi, and L. Shen, "Highly sensitive, reproducible and stable SERS substrate based on reduced graphene oxide/silver nanoparticles coated weighing paper," Appl. Surf. Sci. **404**(15), 334–341 (2017).
36. A. Yz, W. A. Long, B. Hy, and A. Zl, "Enzyme induced molecularly imprinted polymer on SERS substrate for ultrasensitive detection of patulin," Anal. Chim. Acta **1101**, 111–119 (2020).
37. G. L. Long and J. D. Winefordner, "Limit of detection. A closer look at the IUPAC definition," Anal. Chem. **55**(7), 712A–724A (1983).
38. J. A. Dieringer, A. D. Mcfarland, N. C. Shah, and S. Douglas, "Surface enhanced Raman spectroscopy: new materials, concepts, characterization tools, and applications," Faraday Discuss. **132**(2), 9–26 (2006).
39. T. Xue, X. Cui, J. Chen, and C. Liu, "A switch of the oxidation state of graphene oxide on a surface plasmon resonance chip," ACS Appl. Mater. Interfaces **5**(6), 2096–2103 (2013).
40. J. N. Yih, S. J. Chen, and K. T. Huang, "A compact surface plasmon resonance and surface-enhanced Raman scattering sensing device," Int. Society Opt. **5327**, 5–9 (2004).
41. G. Xu, M. Tazawa, P. Jin, and S. Nakao, "Wavelength tuning of surface plasmon resonance using dielectric layers on silver island films," Appl. Phys. Lett. **82**(22), 3811–3813 (2003).
42. M. Moskovits, "Surface-enhanced Raman spectroscopy: a brief retrospective," J. Raman Spectrosc. **36**(6-7), 485–496 (2005).
43. R. Li, G. Yang, and J. Yang, "Determination of melamine in milk using surface plasma effect of aggregated Au@SiO2 nanoparticles by SERS technique," Food Control **68**, 14–19 (2016).
44. K. Kolwas, A. Derkachova, and M. Shopa, "Size characteristics of surface plasmons and their manifestation in scattering properties of metal particles," J. Quant. Spectrosc. Radiat. Transf. **110**(14-16), 1490–1501 (2009).
45. P. N. Njoki, I. Lim, D. Mott, and H. Y. Park, "Size Correlation of Optical and Spectroscopic Properties for Gold Nanoparticles," J. Phys. Chem. C **111**(40), 14664–14669 (2007).
46. G. Upender, R. Satyavathi, B. Raju, and K. S. Alee, "Silver nanocluster films as novel SERS substrates for ultrasensitive detection of molecules," Chem. Phys. Lett. **511**(4-6), 309–314 (2011).
47. M. V. Canamares, C. Chenal, R. L. Birke, J. R. Lombardi, and L. B. Rdi, "DFT, SERS, and single-molecule SERS of crystal violet," J. Phys. Chem. C **112**(51), 20295–20300 (2008).
48. C. Jing and F. Yan, "Experimental (SERS) and theoretical (DFT) studies on the adsorption behaviors of l-cysteine on gold/silver nanoparticles," Chem. Phys. Lett. **332**(1), 27–32 (2007).
49. H. Da, H. Jian, and L. Hui, "Fabrication of Au@Ag core-shell NPs as enhanced CT contrast agents with broad antibacterial properties," Colloids Surf., B **117**(1), 29–35 (2014).
50. L. Budakova, H. Brozmanova, and M. Grundmann, "Simultaneous determination of antiepileptic drugs and their two active metabolites by HPLC," J. Sep. Science **31**(1), 1–8 (2008).
51. X. S. Miao and C. D. Metcalfe, "Determination of carbamazepine and its metabolites in aqueous samples using liquid chromatography-electrospray tandem mass spectrometry," Anal. Chem. **75**(15), 3731–3738 (2003).
52. A. M. Tsatsakis, T. K. Psillakis, M. N. Tzatzarakis, and H. Kourtopoulos, "Carbamazepine levels in the hair of patients under long-term treatment: A preliminary study," Clin. Chim. Acta **263**(2), 187–195 (1997).
53. J. Hermida, M. D. Boveda, F. J. Vadillo, and J. C. Tutor, "Comparison between the Cobas Integra immunoassay and high-performance liquid chromatography for therapeutic monitoring of carbamazepine," Clin. Biochem. **35**(3), 251–254 (2002).